*Desalination and Water Treatment*
www.deswater.com
doi: 10.1080/19443994.2014.959062

56 (2015) 2246–2257
November

Taylor & Francis
Taylor & Francis Group

# Development, application, and evaluation of artificial neural network in investigating the removal efficiency of Acid Red 57 by synthesized mesoporous carbon-coated monoliths

Mohamad Rasool Malekbala[a], Soraya Hosseini[a], Salman Masoudi Soltani[b], Rahele Malekbala[c], Thomas S.Y. Choong[a,*], Farahnaz Eghbali Babadi[a]

[a]*Department of Chemical and Environmental Engineering, Universiti Putra Malaysia, 43400 UPM, Serdang, Selangor, Malaysia, Tel. +603 89466293; email: mrmalekbala@gmail.com (M.R. Malekbala), Tel. +60176515750; email: soraya@eng.ukm.my (S. Hosseini), Tel. +603 89466293; Fax: +603 86567120; email: csthomas@upm.edu.my (T.S.Y. Choong), Tel. +601054646993; email: f_eghbali_b@yahoo.com (F.E. Babadi)*
[b]*Division of Energy and Sustainability, Faculty of Engineering, The University of Nottingham, University Park, Nottingham NG7 2RD, UK, Tel. +44 07831610837; email: salman.masoudi_soltani@nottingham.ac.uk (S. Masoudi Soltani)*
[c]*Science and Research Branch, Young Researchers Club, Islamic Azad University, Tehran, Iran, Tel. +603 87495100; email: rahelemalekbala@yahoo.com (R. Malekbala)*

Received 13 December 2013; Accepted 19 August 2014

ABSTRACT

Acid Red 57 (AR57) has been successfully removed from aqueous solution by adsorption on our synthesized mesoporous carbon-coated monolith (MCCM). For the first time, a powerful artificial neural network (ANN) model has been developed to predict the removal efficiency of AR57 on MCCM. Three critical parameters in adsorption systems, that is, solution's initial pH, initial dye concentration, and contact time were incorporated in the ANN model in order to optimize the observed adsorption process. Langmuir and Freundlich adsorption models were then fitted to the adsorption data to estimate the adsorption capacity. It was concluded that Langmuir isotherm was best-fitted to the data showing a maximum monolayer adsorption capacity of 1,162.7 mg/g. The pseudo-first-order and pseudo-second-order kinetic models were subsequently tested to evaluate the kinetics of the adsorption process. It was revealed that the adsorption kinetics could be better represented by the pseudo-second-order model. A comparison was finally drawn between ANN and pseudo-second-order kinetic models. Based on the error analyses and determination of coefficients, ANN was the more appropriate model to describe the studied adsorption process.

*Keywords:* Mesoporous carbon-coated monolith; Adsorption; Artificial neural network; Acid Red 57

## 1. Introduction

The discharge of colored waste materials into receiving streams not only influences the aesthetic nature but also interferes with the transmission of sunlight into streams and therefore minimizes photosynthetic activity of marine species. This has triggered significant consideration to eliminate pollutant dyes from wastewaters during the last few years. Dyes can be classified as anionic (direct, acid, and reactive dyes), cationic (basic

*Corresponding author.

dyes), and non-ionic (disperse dyes) [1,2]. The Acid Red 57 (AR57; anionic dye) is mainly used for dyeing nylon fabrics and coloring leather. Among numerous water treatment methods, adsorption provides a desirable option due to its low initial cost, ease of process, simple design, and flexibility. Carbon materials, for example, activated carbons [3], activated carbon fibers [4], and mesoporous carbon [5] are well-known adsorbents that are applied in the adsorption processes. Activated carbon offers high surface area and a decent degree of surface reactivity. It comprises microporous structures [6], along with high efficiency in the removal of low molecular weight compounds [7]. Microporosity of activated carbon limits its efficient application for the removal of bulky dye molecules with sizes larger than 2 nm. Several researchers have reported that just 14% of pores may be occupied during the adsorption of dyes using activated carbon [8]. The improvement in mesopores over the surface of carbon could possibly improve the adsorption of larger molecules including dyes [5,9]. In order to synthesize an efficient adsorbent for the removal of large molecules such as dyes, mesoporous carbon with the highly mesoporous structure and uniform pore size (from 2 to 50 nm) is desirable. It has been stated that mesoporous carbon has an excellent performance in the adsorption of bulky dye molecules [10,11].

Adsorption processes are strongly dependent on a number of operating factors including solution pH, dye concentration in the solution, temperature of the solution, and the contact time between the adsorbent and the adsorbate in the solution. In a typical adsorption process, multi-input (e.g. pH value, dye concentration, temperature, and contact time) and multi-output (e.g. percentage value of removal, dye adsorbed per unit of adsorbent at time t and at equilibrium) variables are closely inter-influencing one another. In order to effectively assess the effect of several operational parameters on the adsorption performance and thus model the entire adsorption process, an advanced artificial neural network (ANN) model can be developed [12]. Unfortunately, there are only few reports on modeling dye adsorption by applying ANN. Based on this fact, this research work has tried to develop an ANN model in order to study the effects of experimental parameters on adsorption efficiency of dye molecules in solution.

The ANN is an artificial intelligence approach that mimics the human brain's biological neural network in the process of solving problems. In this technique, information processes are based upon the framework of a biological neural system. ANN is made up of basic processing units known as neurons. ANN is generally comprised of a parallel interconnected structure like input layer of neurons, a number of hidden layers, and output. The objective of this research was to investigate the feasibility of mesoporous carbon-coated monolith (MCCM) as adsorbent for the removal of AR57. In the previous works, MCCM was used in order to adsorb methylene blue (cationic, basic dye) and methyl orange (anionic, azo reactive dye) with adsorption capacities 388 and 323 mg/g, respectively [9]. The novelty of this work is based on the understanding of intrinsic properties of dyes as adsorbate on adsorption process using MCCM. In the present study, an acid dye was selected as adsorbate and mesoporous carbon-coated monolith (MCCM) was prepared and utilized as an attractive adsorbent for the removal of AR57 from aqueous solution. Next, the effects of various operational parameters, such as initial solution pH, initial dye concentration, and contact time, on the removal of AR57 were investigated. In order to further understand the adsorption process, some isotherm models were also studied. Based on batch adsorption experiments, a three-layer ANN model using a back-propagation algorithm was employed to predict the AR57 removal efficiency by the synthesized MCCM as the adsorbent. Finally, the results obtained from the models were compared with the experimental data.

## 2. Experimental

### 2.1. Chemicals and materials

MCCM was used as the adsorbent. The cordierite monolith (channel width: $1.02 \pm 0.02$ mm and wall thickness: $0.25 \pm 0.02$ mm) was used as a precursor material for the preparation of MCCM. The cordierite monoliths were purchased from Beihai Haihuang Chemical Packing Co. Ltd, China. The chemicals used for the synthesis of mesoporous carbon were furfuryl alcohol (FA; Aldrich, 98%) as the carbon source, pyrrole (Py; Aldrich, 98%) as the binder, nitric acid ($HNO_3$; Aldrich, 65%) as the carbonization catalyst, ethanol ($C_2H_5OH$; Aldrich, 95%), and triblock copolymer pluronic F127 (Aldrich, 99%) as the template ($EO_{106}PO_{70}EO_{106}$, MW: 12.600). AR57 ($C_{24}H_{22}N_4O_6S_2$; 526.58 g/mol) was purchased from Sigma–Aldrich and was used as the adsorbate. All the chemicals and reagents used were of analytical grade or as reported.

### 2.2. Preparation of adsorbent and adsorbate

MCCM was prepared by employing dip coating method [13]. This method consists of dipping the cordierite monolith into a liquid polymer that is subsequently cross-linked and carbonized. In order to prepare the polymer solution, non-ionic surfactant

was dissolved in 10 mL $C_2H_5OH$ under continuous stirring at 25˚C. FA, our carbon source, and pyrrole as the binder were added thereafter. The resulting mixture was stirred for 30 min in an ice bath. After that, $HNO_3$ (a catalyst) was added, and the mixture was continuously stirred for an hour resulting in a dark red-colored solution. The dried cordierite monolith was then thoroughly soaked in the viscous polymerized mixture for 20 min. Air with a pressure of 4 kg/cm$^2$ was passed through the monolith channels to remove the excessive coating solution (preventing channels blockage). The solidification of brown monolith was done by heating it at 110˚C for 24 h. The monolith was then carbonized at 700˚C for 4 h under $N_2$ atmosphere at a heating rate of 3˚C/min. The synthesized monolith was then labeled as MCCM. To avoid moisture uptake, the derived MCCM was stored in a desiccator.

The stock dye solution was prepared by dissolving 1 g of dye in 1 L of distilled water. Experimental solutions of desired concentration were obtained by further dilutions from the stock solution. The chemical structure of AR57 is illustrated in Fig. 1.

### 2.3. Analytical method

The concentration of AR57 in aqueous phase before and after adsorption was measured by UV–visible spectrophotometer (Ultrospec$^{TM}$ 3100p). The maximum wavelength ($\lambda_{max}$) for AR57 absorbance as determined by UV–visible spectrophotometer was 517 nm. The pH of the solutions during these studies was determined by a pH meter (Schott instruments).

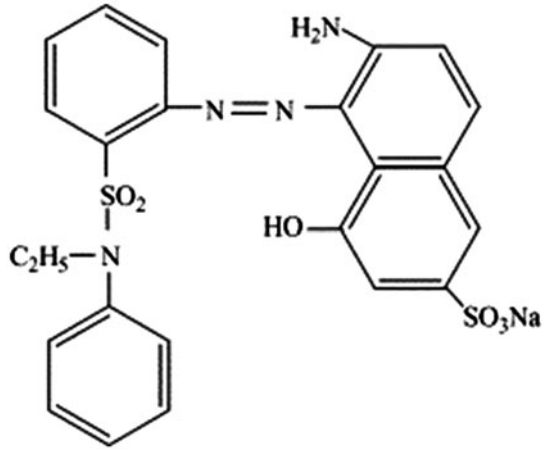


Fig. 1. The chemical structure of AR57.

### 2.4. Characterization of adsorbent

The nitrogen adsorption/desorption isotherm of MCCM was measured using a Sorptomatic v1.03. The surface area and pores size distributions were calculated using the Brunauer–Emmet–Teller and Brunauer–Joyner–Halenda models, respectively. A Perkin Elmer Spectrum (100 FT-IR Spectrometer) with PIKE MIRacle attenuated total reflection attachment was used to record the spectra of MCCM in the range of 4,000–600 cm$^{-1}$. The surface morphology of monolith was observed by a scanning electron microscope (SEM) (Hitachi Co., Japan, Model No. S3400 N).

The acidic and basic sites present on MCCM surface were determined by acid–base titration experiments [14]. The total acidic sites were neutralized using alkaline solutions (0.1 M NaOH, 0.1 M $NaHCO_3$, 0.1 M $Na_2CO_3$, and 0.1 M $NaOC_2H_5$), while basic sites were neutralized with a 0.1 M HCl solution. The acidic and basic sites were determined by adding 50 mL of 0.1 M titrating solutions and 0.5 g of MCCM to each 250-mL volumetric flasks. The flasks were slowly agitated in a temperature-controlled water bath at 25˚C and were left stirred for 5 d. Afterward, 10 mL of each sample was titrated with 0.1 M HCl or 0.1 M NaOH solutions. The titration was carried out in triplicates using a potentiometer.

### 2.5. Batch adsorption studies

A series of batch adsorption experiments was conducted to determine the effect of initial pH (2–11), initial concentration (100–800 mg/L), and contact time (0–4,480 min) on the adsorptive performance of MCCM. Studies were carried out in 250-mL volumetric flasks containing 200 mL of AR57 dye (adsorbate) solution. The adsorbate solution was equilibrated with 0.5 g adsorbent in a shaker at 200 rpm at ambient temperature. The adsorption capacity at the equilibrium ($q_e$) was calculated as:

$$q_e = (C_0 - C_e)\frac{V}{m} \quad (1)$$

where $C_0$ and $C_e$ are the initial and equilibrium adsorbate concentrations (mg/L), respectively. $V$ is the volume of solution (L), and $m$ is the mass of adsorbent (g).

### 2.6. Adsorption isotherms

The adsorption equilibrium is the most critical part of the experimental information to evaluate the

adsorption process. Over the present study, two-parameter Langmuir and Freundlich isotherm models were applied to the equilibrium data. Langmuir isotherm in its linearized form is given as [15]:

$$\frac{C_e}{q_e} = \frac{1}{K_L} + \frac{a_L C_e}{K_L} \tag{2}$$

where $C_e$ (mg/L) and $q_e$ (mg/g) are the equilibrium concentration and the adsorption capacity at equilibrium state, respectively. The Langmuir isotherm constants $a_L$ (L/mg) and $K_L$ (L/g) are obtained from the intercept and slope of the plot of $C_e/q_e$ against $C_e$. The essential feature of Langmuir isotherm can be expressed by separation factor ($R_L$), a dimensionless constant that can be represented as [16]:

$$R_L = \frac{1}{1 + K_L C_0} \tag{3}$$

where if $R_L = 0$, then the adsorption process is irreversible, $0 < R_L < 1$, then the adsorption process is favorable, $R_L = 1$, then the adsorption process is linear, $R_L > 1$, then the adsorption process is unfavorable

A linear form of the Freundlich model can be written as:

$$\log q_e = \log K_F + \frac{1}{n} \log C_e \tag{4}$$

The constant $K_F$ (mg/g)(L/mg)$^{1/n}$ and exponent $1/n$ can be obtained from the intercepts and the slopes of the linear plots of log $q_e$ against log $C_e$ [17,18].

### 2.7. Adsorption kinetics

Pseudo-first-order and pseudo-second-order models were applied to kinetic data. The pseudo-first-order kinetic model [19] is given as:

$$\log (q_e - q_t) = \log q_e - \frac{k_1}{2.3} \times t \tag{5}$$

where $q_t$ (mg/g) is the amount of dye adsorbed at time $t$ (min) and $k_1$ (1/min) is the pseudo-first-order rate constant. The values of $k_1$ and $q_e$ were determined by plotting log ($q_e - q_t$) against $t$. Pseudo-second-order kinetic model [20] is expressed as:

$$\frac{t}{q_t} = \frac{1}{k_2 q_e^2} + \frac{t}{q_e} \tag{6}$$

where $k_2$ is the pseudo-second-order rate constant. The plot of $t/q_t$ vs. $t$ gives a straight line with a slope of $1/k_2 q_e^2$ and an intercept of $1/q_e$.

### 2.8. Artificial neural network

The development of empirical models by using numerical estimation methods such as ANN can be considered as an effective alternative for predicting adsorption processes. In this study, Neural Network Toolbox V 7.12 of MATLAB mathematical software was used to predict the adsorption efficiency. This multilayered network is a structure consisting of (i) input layer of neuron (independent variables), (ii) a number of hidden layers, and (iii) output layer (dependent variables) [21,22]. The experimental data were separated into input matrix and output matrix. The input variables to the feed-forward neural network were initial adsorbate pH ($pH_i$, 2–5), initial adsorbate concentration ($C_0$, 100–800 mg/L), and contact time ($t$, 0–4,480 min). The output layer had one neuron as the amount of AR57 adsorbed on MCCM.

A three-layer ANN with the tangent sigmoid transfer functions with a back-propagation algorithm at hidden layer and a linear transfer function at output layer transfer functions were used. Tangent sigmoid transfer function is expressed as:

$$f(x) = \frac{1}{1 + \exp^{(-x)}} \tag{7}$$

where $f(x)$ is hidden neuron output.

In this study, 504 experimental mean data points were chosen to feed the ANN structure. The ranges of operating variables were four $pH_i$ values, six initial dye concentrations, and 21 points of contact time. The data samples were divided into three sets training (70%), validation (15%), and testing (15%), respectively. All samples were to be scaled in 0–1 range using sigmoid transfer function in the hidden layer. So, all the data sets ($X_i$) (from the training, validation, and test sets) were scaled to a new value ($x_i$) as follows:

$$x_i = \frac{Xi - X_{\min}}{X_{\max} - X_{\min}} \tag{8}$$

The error function was estimated using mean square error (MSE) as:

$$\mathrm{MSE} = \frac{1}{N} \sum_{i=1}^{n} (q_{\mathrm{predict}} - q_{\mathrm{exp}})^2 \tag{9}$$

where $N$ is the number of data point, $q_{predict}$ is the predicted adsorption data from ANN and pseudo-second-order models and $q_{exp}$ is the observed experimental adsorption data.

## 3. Results and discussion

### 3.1. Characterization of adsorbents

Nitrogen adsorption–desorption isotherm plot of MCCM sample is presented in Fig. 2. According to IUPAC, this isotherm falls under type IV classification, which is typically demonstrating mesoporous materials. The pore area and pore volume were also estimated. The observed total pore area was 849.5 $m^2/g$ inclusive of mesopore area (576.5 $m^2/g$) and micropore area (272.9 $m^2/g$). The total pore volume was calculated to be 0.34 $cm^3/g$ covering both mesopore volume (0.29 $cm^3/g$) and micropore volume (0.05 $cm^3/g$). This shows that about 97% of the total pore volume belongs to the mesopores indicating the dominance of mesopore volume, compared to micropore volume (Figs. 2 and 3). In addition, Boehm titration experiments revealed a larger number of acidic sites over the surface of MCCM (Table 1). This indicates that the acidic functionality dominates over the surface of MCCM.

The FT-IR spectrum of MCCM is presented in Fig. 4. The vibration peaks at 2,991, 2,884, and 2,784 $cm^{-1}$ are assigned to asymmetric and symmetric stretching of $CH_2$ groups [22]. The bands at 1,567 and 1,416 $cm^{-1}$ belong to ring stretching vibrations [23]. In addition, a strong band at 1,182 $cm^{-1}$ confirms the presence of C–O stretching vibrations [24]. The bands at 956, 909, and 770 $cm^{-1}$ assigned to C–H plane bending vibration in the aromatic moiety were also present on MCCM [25]. Intense peak in the higher-energy region also includes O–H stretching of water [26]. Moreover, this could be attributed to pyrolysis and some chemical reactions during carbonization of the material [27].

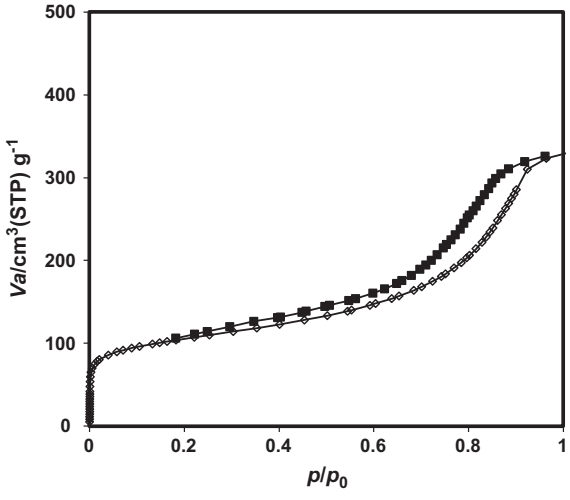


Fig. 2. Nitrogen adsorption/desorption isotherm curves of MCCM.

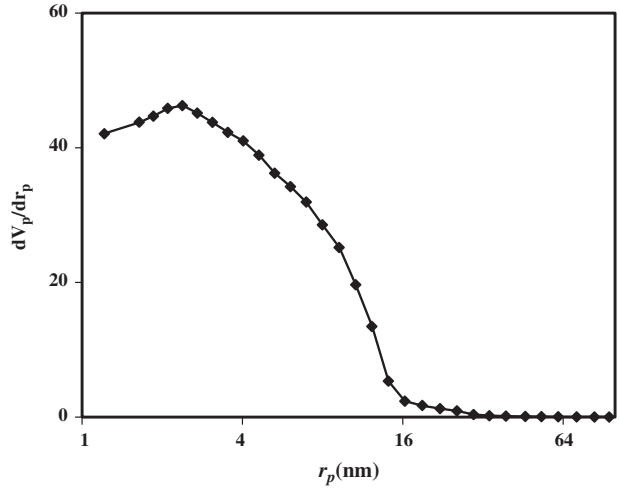


Fig. 3. Pore size distribution of MCCM.

Table 1
Surface active sites on MCCM

| Active sites | Values (millieq./g) |
|---|---|
| *Total acidic sites* | 0.6612 |
| Carboxylic | 0.1651 |
| Lactonic | 0.1277 |
| Phenolic | 0.3684 |
| *Total basic sites* | 0.0205 |

SEM images of mesoporous carbon-coating on honeycomb cordierite after carbonization show relatively uniform surface and the coverage of carbon inside the channels (Fig. 5(c) and (d)). The development of highly porous surface on the covered carbon can be observed in the image with a high magnification (Fig. 5(e)), indicating a high degree of porosity of coated carbon after carbonization.

### 3.2. Effect of initial pH

The effect of pH on AR57 adsorption was studied by varying the pH from 2 to 11 using 200 mg/L initial AR2 concentration at 30°C (Fig. 6). The adsorption of AR57 was found to decrease with an increase in the

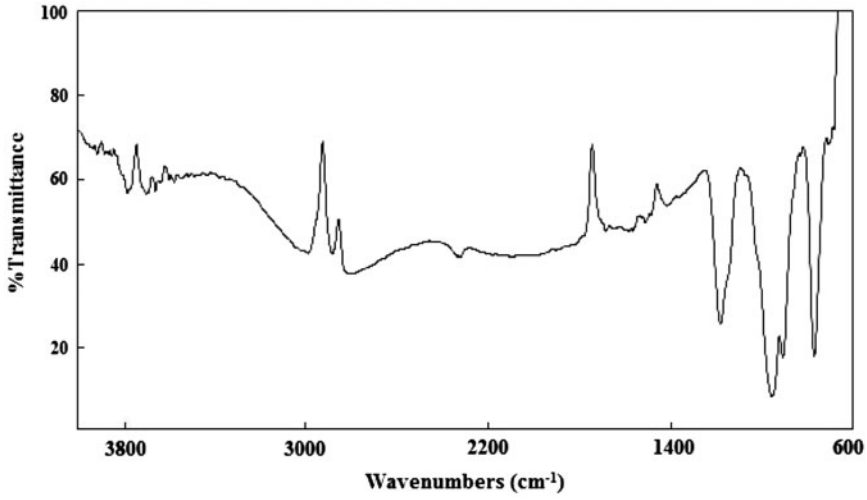


Fig. 4. FT-IR spectra of MCCM.

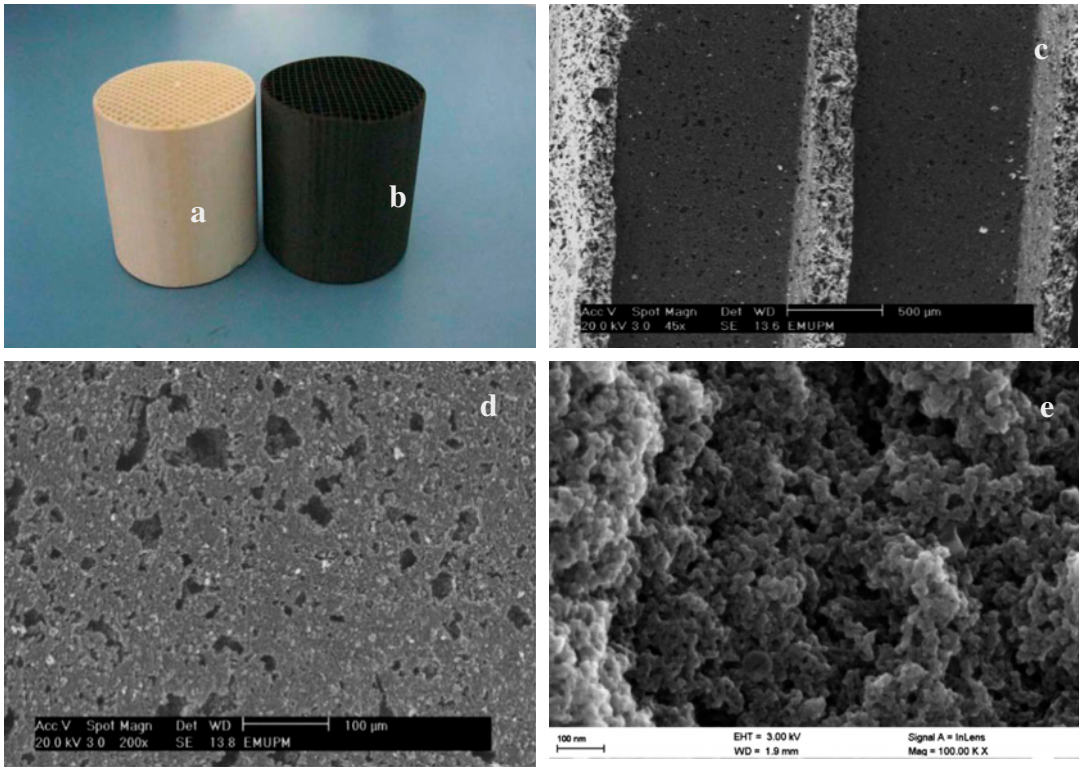


Fig. 5. Optical photos (a) blank cordierite, (b) cordierite after coating with mesoporous carbon, ((c)–(e)) SEM image for mesoporous carbons scraped from cordierite viewed ((c) and (d)) perpendicular, and (e) parallel to the pore channels.

initial pH of the aqueous solution. The amount of dye adsorbed was found to be the highest at pH 2 (432.93 mg/g), whereas the lowest value was observed at pH 11 (321.25 mg/g). Optimum adsorption at lower pH attributed to the existence of higher electrostatic attraction between MCCM surface and anionic dye, AR57. The increase in pH raises the number of negatively charged hydroxyl ions in aqueous phase, causing competition between the excessive hydroxyl ions, and the number of negatively charged dye ions,

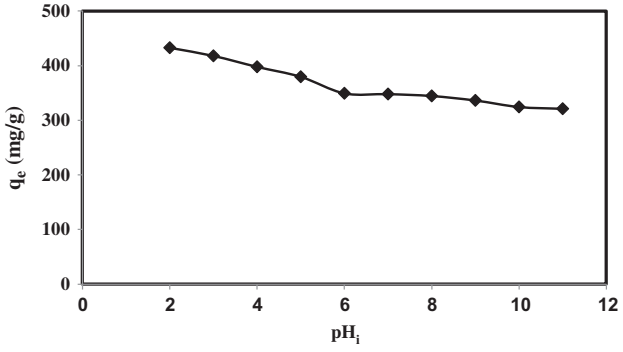


Fig. 6. Effect of pH for the adsorption of AR57 on MCCM. Conditions: initial concentration 200 mg/L, mass of MCCM (0.5 g), speed of shaker (200 rpm), and temperature (30˚C).

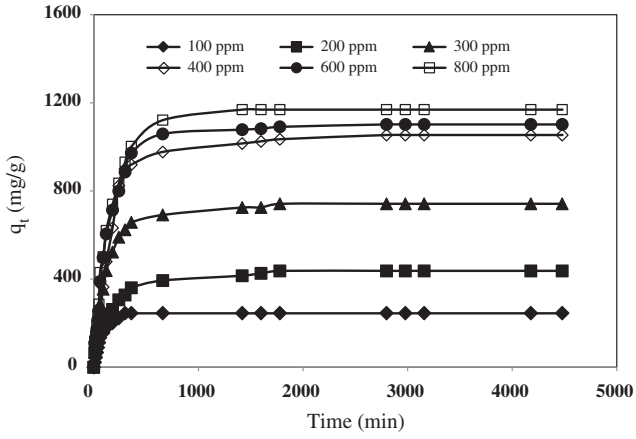


Fig. 7. Effect of contact time for the adsorption of AR57 at various initial concentrations on MCCM. Conditions: mass of MCCM (0.5 g), speed of shaker (200 rpm), and temperature (30˚C).

decreasing adsorption capacity [18]. Therefore, pH 2 was selected as the optimum value for the next studies.

### 3.3. Effect of contact time and initial dye concentration

Contact time experiments were carried out by varying adsorbate concentration from 100 to 800 mg/L. Rapid AR57 uptake was observed for the initial 240 min, which gradually slows down attaining equilibrium between 240 and 1,420 min. The adsorption capacity at equilibrium increased from 245.39 to 1,169.27 mg/g with an increase in initial AR57 concentration from 100 to 800 mg/L, respectively (Fig. 7). This is due to an increase in the driving force of the concentration gradient owing to an increase in the initial dye concentration.

### 3.4. Adsorption isotherm

To optimize the design of an adsorption system, Langmuir and Freundlich isotherm models were applied. The data have been analyzed by correlation coefficients ($R^2$). The coefficients for the Freundlich and Langmuir isotherm analyses are all above 0.97. Comparatively, higher regression coefficient ($R^2$) value

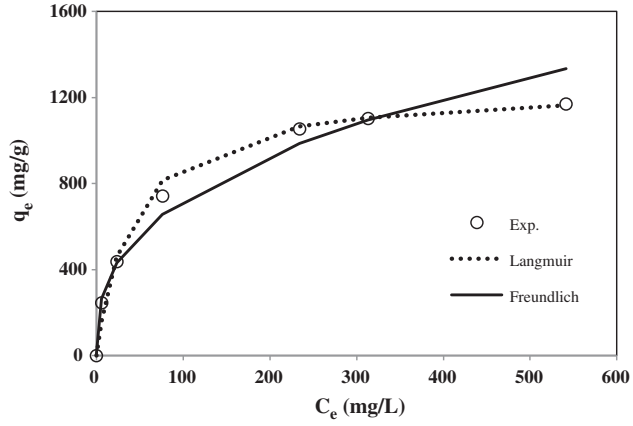


Fig. 8. Non-linear isotherm plots for the adsorption of AR57 on MCCM. Conditions: mass of MCCM (0.5 g), speed of shaker (200 rpm), and temperature (30˚C).

for Langmuir model showed better fitting of the model to the experimental data. This confirms monolayer coverage of AR57 on the MCCM surface and also homogeneous distribution of active sites on the

Table 2
Isotherm parameters for AR57 adsorption onto MCCM

| Langmuir constants | | | Freundlich constants | | |
|---|---|---|---|---|---|
| $K_L$ (L/g) | $q_m$ (mg/g) | $R^2$ | $K_F$ (mg/g)(L/mg)$^{1/n}$ | $1/n$ | $R^2$ |
| 30.8 | 1,162.7 | 0.99 | 137.4 | 0.36 | 0.97 |

Table 3
Comparison of adsorption capacities of various adsorbents for AR57

| Adsorbents | $Q_0$ (mg/g) | References |
|---|---|---|
| MCCM | 1162.7 | This Work |
| CMK-5 | 1,131 | [29] |
| Surfactant-modified sepiolite | 425 | [30] |

adsorbent surface. These results were well evident by non-linear plots (Fig. 8). As shown in Table 2, the maximum adsorption capacity of AR57 was recorded to be 1,162.7 mg/g. The maximum adsorption capacity ($q_0$) of the MCCM was compared with other reported data as shown in Table 3. The performance of the MCCM is seen to be considerably better than other sorbents listed in the table. The essential feature of Langmuir isotherm also confirms that the adoption of

Table 4
Kinetics parameters for AR57 adsorption onto MCCM

| | | Pseudo-first order | | | Pseudo-second order | | |
|---|---|---|---|---|---|---|---|
| $C_0$ (mg/L) | $q_{e,\ exp}$ (mg/g) | $q_{e,cal}$ (mg/g) | $k_1 \times 10^{-4}$ (1/min) | $R^2$ | $q_{e,cal}$ (mg/g) | $k_2 \times 10^{-5}$ (g/mgmin) | $R^2$ |
| 100 | 245.39 | 227.8 | 96.72 | 0.98 | 250.14 | 8.35 | 0.997 |
| 200 | 436.85 | 339.31 | 39.15 | 0.95 | 454.55 | 2.48 | 0.998 |
| 300 | 741.67 | 705.48 | 62.18 | 0.96 | 769.23 | 1.27 | 0.995 |
| 400 | 1,053.4 | 1,035.92 | 64.48 | 0.95 | 1,069.63 | 0.72 | 0.998 |
| 600 | 1,101.89 | 1,079.01 | 52.96 | 0.97 | 1,111.21 | 0.54 | 0.994 |
| 800 | 1,169.27 | 1,130.57 | 50.66 | 0.97 | 1,250.01 | 0.71 | 0.994 |

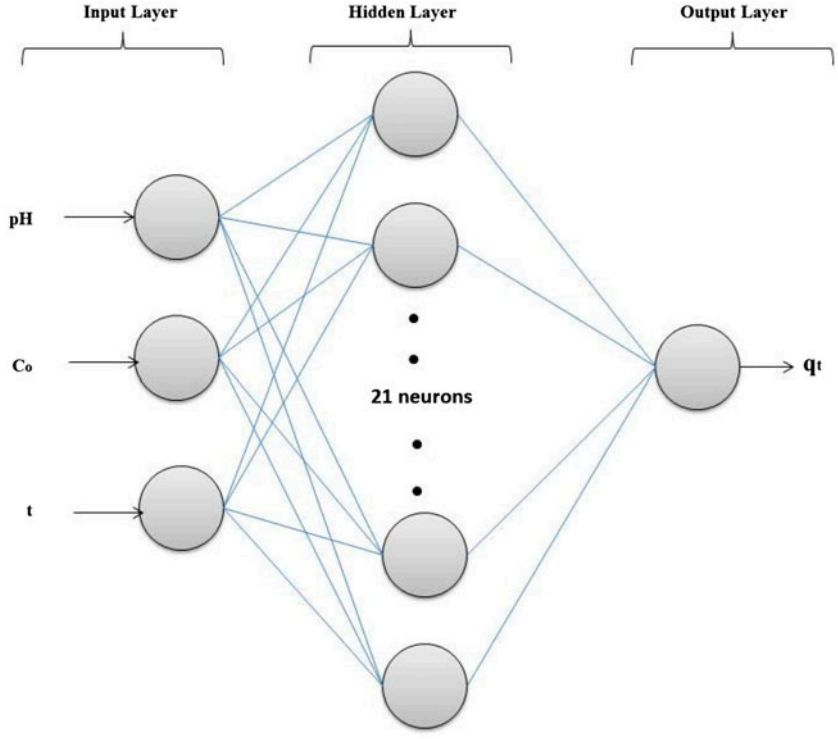


Fig. 9. ANN optimized structure ($pH_i$ = 2–5, $C_0$ = 100–800 mg/L, and $t$ = 0–4,480 min).

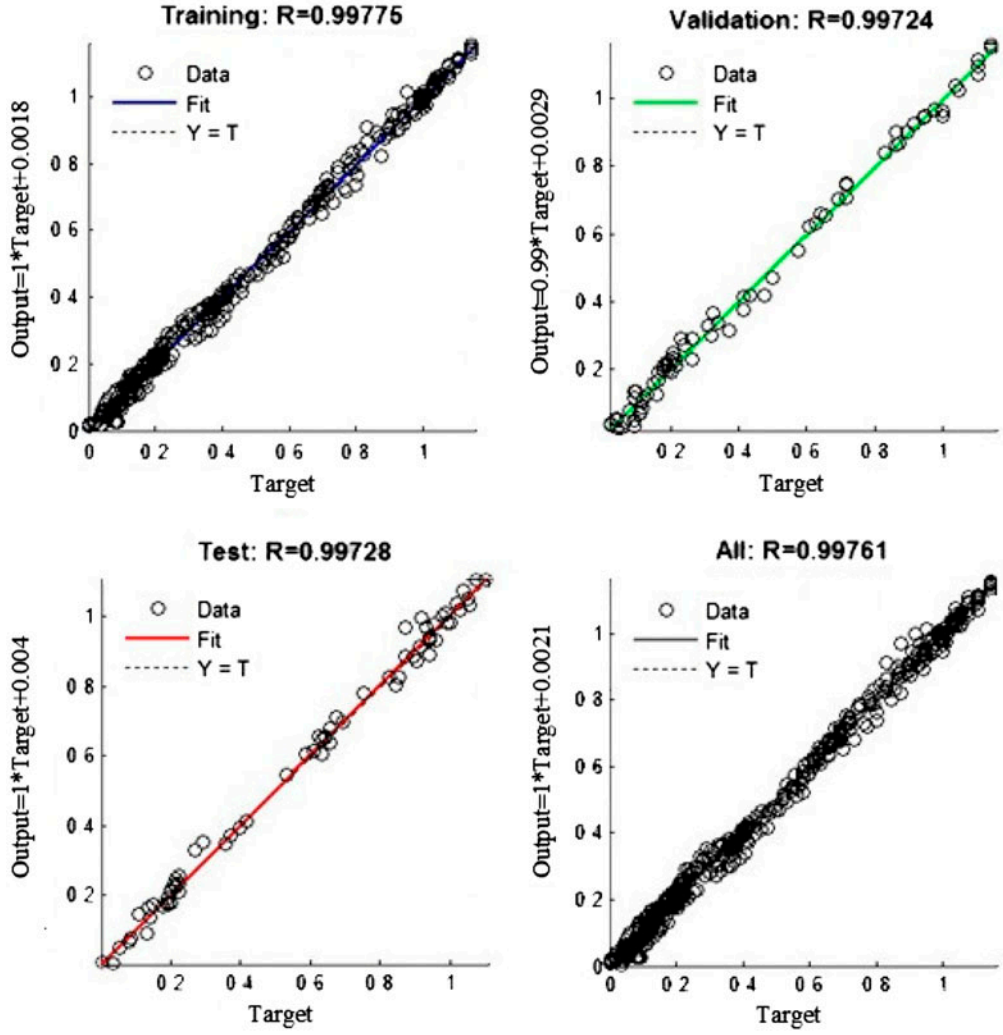


Fig. 10. Network model with training, validation, test, and all prediction set.

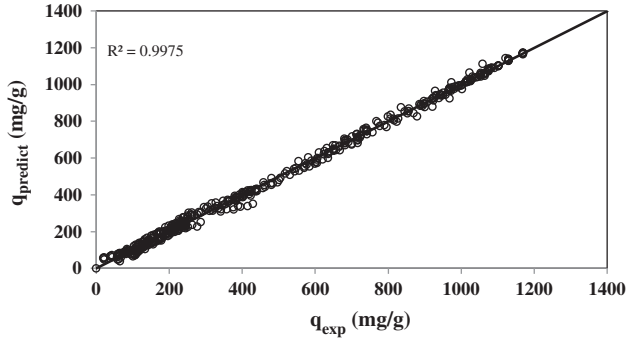


Fig. 11. Comparison of the experimental data with those predicted data from ANN modeling ($pH_i$ = 2–5, $C_0$ = 100–800 mg/L, and $t$ = 0–4,480 min).

AR57 on MCCM is a favorable adsorption process ($0 < R_L < 1$).

### 3.5. Adsorption kinetics

In order to examine the adsorption processes of AR57 on MCCM, two kinetic models, pseudo-first-order and pseudo-second-order model, were studied. The parameters obtained from these models are presented in Table 4. The pseudo-first-order model does not show a good regression coefficient ($R^2$) for the entire concentration range, whereas pseudo-second-order model shows higher $R^2$ values for the whole concentration range. Moreover, the $q_{exp}$ and $q_e$ values for AR57 on MCCM are closer (Table 4) that confirms the applicability of the pseudo-second-order model for

Table 5
Kinetic parameters for the adsorption of AR57 on MCCM (pH$_i$ 2, $C_0$ = 100–800 mg/L, and $t$ = 0–4,480 min)

| | $C_0$ (mg/L) | 100 | 200 | 300 | 400 | 600 | 800 |
|---|---|---|---|---|---|---|---|
| ANN | $q_{exp}$ | 245.39 | 436.85 | 741.67 | 1,053.4 | 1,101.89 | 1,169.27 |
| | $q_{predict}$ | 241.75 | 435.78 | 741.44 | 1,052.46 | 1,101.33 | 1,165.53 |
| | $R^2$ | 0.996 | 0.998 | 0.999 | 0.998 | 0.999 | 0.999 |
| | MSE | 6.6529 | 1.0668 | 4.6529 | 0.9365 | 0.5598 | 3.7425 |
| Pseudo-second | $q_{predict}$ | 250.14 | 454.55 | 769.23 | 1,069.63 | 1,111.21 | 1250.01 |
| | $R^2$ | 0.997 | 0.998 | 0.995 | 0.998 | 0.994 | 0.994 |
| | MSE | 20.5641 | 31.1804 | 43.3362 | 24.6409 | 51.4651 | 66.9318 |

the entire concentration range. The applicability of pseudo-second-order model suggests a chemisorption process in these experiments.

### 3.6. ANN studies

A three-layer ANN with tangent sigmoid transfer function at hidden layer and a linear transfer function at output layer were used in this study. The input layer had three neurons as initial pH, initial dye concentration, and contact time. The output layer had one neuron as the amount of adsorbed AR57 on the MCCM. A series of topologies was utilized to figure out the optimum number of hidden nodes, in which the number of nodes varied from 2 to 25. Based on the approximation of MSE function, a number of hidden neurons equal to 21 were adopted and a three-layer feed-forward back-propagation neural network was used for the modeling of the process (Fig. 9). Fig. 10 shows the regression plots for the output with respect to training, validation, and test data. The output tracks the targets very well, and the $R$-value is over 0.997. In this case, the network response is suitable. Regression analysis of the network response between ANN outputs (predicted, $q_{predict}$) and the corresponding targets (experimental, $q_{exp}$) is illustrated in Fig. 11. It is seen that a larger determination coefficient ($R^2$, 0.997) for data-set has been calculated. The evaluation between ANNs and pseudo-second-order kinetic models were taken to find out the best model for the adsorption of AR57 on MCCM. Parameters obtained from ANN and pseudo-second-order kinetic models are given in Table 5. Both models had decent fittings to experimental data. However, in accordance with the values of determination of coefficient ($R^2$ = 0.996) and MSE (0.9365–6.6529), the ANN was determined to be the more appropriate model to explain the adsorption of AR57 on the MCCM. Moreover, the predicted $q_t$ values from the ANN agreed very well with the experimental $q_t$ values compared to those of the pseudo-second-order kinetic model. These results are in good agreement with earlier reports [22,28,29]. The neural net weight matrix [30] was employed to determine the relative importance of the different input variables on the output variables. Results indicated that the initial dye concentration was the most efficient parameter (48%), followed by contact time (39%) and pH (13%) for the adsorption of AR57 on MCCM. Similar results were reported in a previous study in which the initial dye concentration was believed to be the most important factor [28].

## 4. Conclusions

In this study, a synthesized MCCM for the removal AR57 from aqueous solution was researched. Adsorption of AR57 onto the MCCM followed the Langmuir isotherm model. The monolayer adsorption capacity of MCCM was 1,162.7 mg/g. The results suggested strongly that MCCM might be a suitable adsorbent for the removal of AR57. The effect of various operational parameters revealed that MCCM had a great potential to remove AR57 from aqueous solution at different initial pH values, dye concentrations, and contact time. Simulations based on the ANN model were performed in order to estimate the behavior of the system under different conditions. ANN was found to be an excellent model because of lower SME and higher determination of coefficient values between the network prediction and corresponding experimental data. Results also showed that the initial dye concentration is the most efficient parameter during the adsorption process. It was shown that ANN could effectively reproduce experimental data and predict the behavior of this adsorption process.

## Acknowledgments

The authors would like to gratefully acknowledge Ministry of Education (MOE), Malaysian Government and Universiti Putra Malaysia (UPM) for the financial support of this work (via vot: 9416900).

### List of symbols

$C_0$ — initial concentrations of dye solution (mg/L)
$C_t$ — concentrations of dye solution at time $t$ (mg/L)
$C_e$ — concentrations of dye solution at equilibrium time (mg/L)
$k_1$ — pseudo-first-order rate constant (1/min)
$k_2$ — pseudo-second-order rate constant (mg/gmin)
$K_L$ — Langmuir constant (L/mg)
$K_F$ — Freundlich adsorbent capacity (mg/g(L/mg) $1/n$)
$M$ — mass of adsorbent added to the solution (g)
$n$ — the reciprocal of reaction order
$N$ — the number of data point
$q_t$ — adsorption capacity at time $t$ (mg/g)
$q_e$ — adsorption capacity at equilibrium conditions (mg/g)
$q_m$ — maximum adsorption capacity (mg/g)
$q_{\text{predict}}$ — the predicted adsorption data from ANN (mg/g)
$q_{\text{exp}}$ — the observed experimental adsorption data (mg/g)
$R_L$ — dimensionless group
$t$ — time (min)
$V$ — volume of the dye solution (L)

## References

[1] W. Cheah, S. Hosseini, M.A. Khan, T.G. Chuah, T.S.Y. Choong, Acid modified carbon coated monolith for methyl orange adsorption, Chem. Eng. J. 215–216 (2013) 747–754.
[2] S. Hosseini, T.S.Y. Choong, M. Hamid, Adsorption of a cationic dye from aqueous solution on mesoporous carbon based honeycomb monolith, Desalin. Water Treat. 49 (2012) 326–336.
[3] V. Meshko, L. Markovska, M. Mincheva, A.E. Rodrigues, Adsorption of basic dyes on granular activated carbon and natural zeolite, Water Res. 35 (2001) 3357–3366.
[4] P. Georgiou, J. Walton, J. Simitzis, Surface modification of pyrolyzed carbon fibers by cyclic voltammetry and their characterization with XPS and dye adsorption, Electrochim. Acta 55 (2010) 1207–1216.
[5] S. Hosseini, M.A. Khan, M.R. Malekbala, W. Cheah, T.S.Y. Choong, Carbon coated monolith, a mesoporous material for the removal of methyl orange from aqueous phase: Adsorption and desorption studies, Chem. Eng. J. 171 (2011) 1124–1131.
[6] Y. Dong, H. Lin, F. Qu, Synthesis of ferromagnetic ordered mesoporous carbons for bulky dye molecules adsorption, Chem. Eng. J. 193–194 (2012) 169–177.
[7] L.R. Radovic, I.F. Silva, J.I. Ume, J.A. Menéndez, Y. Leon, A.W. Scaroni, An experimental and theoretical study of the adsorption of aromatics possessing electron-withdrawing and electron-donating functional groups by chemically modified activated carbons, Carbon 35 (1997) 1339–1348.
[8] G.M. Walker, L.R. Weatherley, Adsorption of dyes from aqueous solution—The effect of adsorbent pore size distribution and dye aggregation, Chem. Eng. J. 83 (2001) 201–206.
[9] M.R. Malekbala, M.A. Khan, S. Hosseini, L.C. Abdullah, T.S.Y. Choong, Adsorption/desorption of cationic dye on surfactant modified mesoporous carbon coated monolith: Equilibrium, kinetic and thermodynamic studies, J. Ind. Eng. Chem., doi: 10.1016/j.jiec.2014.02.047.
[10] Z.L. Wang, X.J. Liu, M.F. Lv, J. Meng, Simple synthesis of magnetic mesoporous FeNi/carbon composites with a large capacity for the immobilization of biomolecules, Carbon 48 (2010) 3182–3189.
[11] X. Zhuang, Y. Wan, C.M. Feng, Y. Shen, D.Y. Zhao, Highly efficient adsorption of bulky dye molecules in wastewater on ordered mesoporous carbons, Chem. Mater. 21 (2009) 706–716.
[12] A.R. Khataee, M.B. Kasiri, Artificial neural networks modeling of contaminated water treatment processes by homogeneous and heterogeneous nanocatalysis, J. Mol. Catal. A: Chem. 331 (2010) 86–100.
[13] S. Masoudi Soltani, S. Hosseini, M.R. Malekbala, A review on monolithic honeycomb structures and fabrication techniques, J. Appl. Sci. Res. 9 (2013) 2548–2560.
[14] S.L. Goertzen, K.D. Thériault, A.M. Oickle, A.C. Tarasuk, H.A. Andreas, Standardization of the Boehm titration. Part I: $CO_2$ expulsion and endpoint determination, Carbon 48 (2010) 1252–1261.
[15] G. Crini, H.N. Peindy, F. Gimbert, C. Robert, Removal of C.I. Basic Green 4 (Malachite Green) from aqueous solutions by adsorption using cyclodextrin-based adsorbent: Kinetic and equilibrium studies, Sep. Purif. Technol. 53 (2007) 97–110.
[16] M. Iram, C. Guo, Y. Guan, A. Ishfaq, H. Liu, Adsorption and magnetic removal of neutral red dye from aqueous solution using Fe3O4 hollow nanospheres, J. Hazard. Mater. 181 (2010) 1039–1050.
[17] S.D. Khattri, M.K. Singh, Removal of malachite green from dye wastewater using neem sawdust by adsorption, J. Hazard. Mater. 167 (2009) 1089–1094.
[18] I. Kiran, T. Akar, A.S. Ozcan, A. Ozcan, S. Tunali, Biosorption kinetics and isotherm studies of Acid Red 57 by dried *Cephalosporium aphidicola* cells from aqueous solutions, Biochem. Eng. J. 31 (2006) 197–203.
[19] X. Peng, D. Huang, T. Odoom-Wubah, D. Fu, J. Huang, Q. Qin, Adsorption of anionic and cationic dyes on ferromagnetic ordered mesoporous carbon from aqueous solution: Equilibrium, thermodynamic and kinetics, J. Colloid Interface Sci. 430 (2014) 272–282.
[20] W.C. Wanyonyi, J.M. Onyari, P.M. Shiundu, Adsorption of Congo Red Dye from aqueous solutions using roots of *Eichhornia crassipes*: Kinetic and equilibrium studies, Energy Procedia 50 (2014) 862–869.
[21] A.R. Khataee, M. Zarei, G. Dehghan, E. Ebadi, M. Pourhassan, Biotreatment of a triphenylmethane dye solution using a Xanthophyta alga: Modeling of key factors by neural network, J. Taiwan Inst. Chem. E. 42 (2011) 380–386.

[22] A. Çelekli, F. Geyik, Artificial neural networks (ANN) approach for modeling of removal of Lanaset Red G on *Chara contraria*, Bioresour. Technol. 102 (2011) 5634–5638.
[23] N.F. Cardoso, R.B. Pinto, E.C. Lima, T.C. Calvete, C.V. Amavisca, B. Royer, M.L. Cunha, T.H.M. Fernandes, I.S. Pinto, Removal of remazol black B textile dye from aqueous solution by adsorption, Desalination 269 (2011) 92–103.
[24] D. Sidiras, F. Batzias, E. Schroeder, R. Ranjan, M. Tsapatsis, Dye adsorption on autohydrolyzed pine sawdust in batch and fixed-bed systems, Chem. Eng. J. 171 (2011) 883–896.
[25] B.K. Nandi, A. Goswami, M.K. Purkait, Removal of cationic dyes from aqueous solutions by kaolin: Kinetic and equilibrium studies, Appl. Clay Sci. 42 (2009) 583–590.
[26] C.K. How, M.A. Khan, S. Hosseini, T.G. Chuah, T.S.Y. Choong, Fabrication of mesoporous carbons coated monolith via evaporative induced self-assembly approach: Effect of solvent and acid concentration on pore architecture, J. Ind. Eng. Chem., doi: 10.1016/j.jiec.2014.01.034.
[27] K. Muthukumaran, S.S. Beulah, SEM and FT-IR Studies on nature of adsorption of mercury(II) and chromium(VI) from wastewater using chemically activated syzygium jambolanum nut carbon, Asian J. Chem. 22 (2010) 7857–7864.
[28] M. Auta, B.H. Hameed, Preparation of waste tea activated carbon using potassium acetate as an activating agent for adsorption of Acid Blue 25 dye, Chem. Eng. J. 171 (2011) 502–509.
[29] A.R. Khataee, G. Dehghan, M. Zarei, E. Ebadi, M. Pourhassan, Neural network modeling of biotreatment of triphenylmethane dye solution by a green macroalgae, Chem. Eng. Res. Des. 89 (2011) 172–178.
[30] Y. Yang, G. Wang, B. Wang, Z. Li, X. Jia, Q. Zhou, Y. Zhao, Biosorption of Acid Black 172 and Congo Red from aqueous solution by nonviable Penicillium YW 01: Kinetic study, equilibrium isotherm and artificial neural network modeling, Bioresour. Technol. 102 (2011) 828–834.